LETTER

doi:10.1038/nature21383

Earth's first stable continents did not form by subduction

Tim E. Johnson[1], Michael Brown[2], Nicholas J. Gardiner[1], Christopher L. Kirkland[1] & R. Hugh Smithies[3]

The geodynamic environment in which Earth's first continents formed and were stabilized remains controversial[1]. Most exposed continental crust that can be dated back to the Archaean eon (4 billion to 2.5 billion years ago) comprises tonalite–trondhjemite–granodiorite rocks (TTGs) that were formed through partial melting of hydrated low-magnesium basaltic rocks[2]; notably, these TTGs have 'arc-like' signatures of trace elements and thus resemble the continental crust produced in modern subduction settings[3]. In the East Pilbara Terrane, Western Australia, low-magnesium basalts of the Coucal Formation at the base of the Pilbara Supergroup have trace-element compositions that are consistent with these being source rocks for TTGs. These basalts may be the remnants of a thick (more than 35 kilometres thick), ancient (more than 3.5 billion years old) basaltic crust[4,5] that is predicted to have existed if Archaean mantle temperatures were much hotter than today's[6–8]. Here, using phase equilibria modelling of the Coucal basalts, we confirm their suitability as TTG 'parents', and suggest that TTGs were produced by around 20 per cent to 30 per cent melting of the Coucal basalts along high geothermal gradients (of more than 700 degrees Celsius per gigapascal). We also analyse the trace-element composition of the Coucal basalts, and propose that these rocks were themselves derived from an earlier generation of high-magnesium basaltic rocks, suggesting that the arc-like signature in Archaean TTGs was inherited from an ancestral source lineage. This protracted, multistage process for the production and stabilization of the first continents—coupled with the high geothermal gradients—is incompatible with modern-style plate tectonics, and favours instead the formation of TTGs near the base of thick, plateau-like basaltic crust[9]. Thus subduction was not required to produce TTGs in the early Archaean eon.

Eoarchaean to Palaeoarchaean TTGs (dating back 4.0 billion years to 3.2 billion years, Gyr) form the earliest cratons[1]—the ancient nuclei of continents. Establishing how these TTGs formed is key to understanding how continental crust formed and stabilized. TTGs are variably deformed and metamorphosed felsic igneous rocks, rich in silica (average 69 wt%), aluminium oxide (around 15 wt%) and sodium oxide (3–7 wt%), and are characterized by low potassium oxide/sodium oxide ratios (averaging around 0.4) and high strontium/yttrium (Sr/Y) ratios (averaging about 40)[4,10]. Although there is consensus that TTGs formed by partial melting of hydrated basaltic rocks[11,12], there remains considerable controversy surrounding the geodynamic setting, with implications for our understanding of early Earth evolution. Models for producing Archaean continental crust generally fall into two camps: those that invoke plate tectonics, and those that do not. Uniformitarian models, which involve plate tectonics and a dominance of horizontal forces, suggest that TTGs formed by partial melting of a subducting slab, as do modern-day adakites[3,12,13]. Non-uniformitarian models, in which vertical forces were dominant, instead propose that TTGs were produced near the base of thick, plateau-like mafic crust, whose formation was coupled to that of buoyant, subcontinental mantle lithosphere that was highly depleted in crust-forming components[9,14–16].

TTGs have been classified into low-, medium- and high-pressure variants on the basis of partial melting experiments using amphibolite, metamorphic rocks dominated by amphibole (hornblende) and plagioclase[10,17]. Low-pressure TTGs (LP-TTGs) have relatively low Sr/Y ratios, consistent with melt residues that are rich in plagioclase (which sequesters strontium) but with little or no garnet (which sequesters yttrium and heavy rare-earth elements, HREEs); LP-TTGs are inferred to have formed at pressures of 1.0–1.2 GPa (at about 30–35 km depth)[10]. Medium-pressure TTGs (MP-TTGs) have moderate to high Sr/Y ratios and formed in equilibrium with residues that are rich in garnet, but with little or no rutile (which sequesters niobium (Nb) and tantalum (Ta)) or plagioclase; this is interpreted to reflect melting at a pressure of about 1.5 GPa (around 45 km depth)[10]. High-pressure TTGs (HP-TTGs) have high Sr/Y and lanthanum/niobium (La/Nb) ratios; such ratios are thought to reflect residues that are rich in garnet and rutile but lack plagioclase, and which are considered to have formed at pressures greater than 2.0 GPa (at about 60 km depth)[10]. Thus, the trace-element composition of TTGs can be used to infer the depth of melting of their source rocks, with implications for discriminating the geodynamic environment in which they formed[18].

To help resolve the geodynamic provenance of early Archaean TTGs, we use new thermodynamic models that are applicable to mafic rocks[19] to model the partial melting of a putative Palaeoarchaean TTG basaltic source. Phase equilibria modelling permits the calculation of the abundance and composition of minerals, volatile species and melt as a function of pressure, temperature and bulk rock composition. We couple this modelling with trace-element geochemistry to predict conditions of melting and to infer a likely geodynamic setting for the formation of TTGs and the generation of Earth's first stable continents.

The East Pilbara Terrane, part of the Pilbara Craton in Western Australia, is among the oldest remnants of Earth's Archaean continental nuclei[20]. It is volumetrically dominated by Palaeoarchaean TTGs whose compositions require source rocks that are much more enriched in thorium, large-ion lithophile elements (LILEs) and light rare-earth elements (LREEs) than are mid-ocean-ridge basalt (MORB) or many Archaean basalts[4]. However, 3.5-Gyr-old basalts and basaltic andesites within the Coucal Formation (hereafter Coucal basalts), at the base of the Pilbara Supergroup, have been shown to be suitable source rocks for the East Pilbara TTGs, at least in terms of their trace-element compositions, and may have formed a large proportion of a pre-3.5-Gyr-ago mafic protocrust that was 35 km or more in thickness[4]. Such rocks are not unique to the Pilbara—Palaeoarchaean TTGs and enriched basalts also occur in the Barberton greenstone belt in southern Africa, and probably formed in a similar setting[21].

The Coucal basalts (Extended Data Table 1) form a tholeiitic series that is characterized by substantial enrichment in incompatible trace elements relative to enriched (E)-MORB, to normal (N)-MORB and to other Pilbara Supergroup basalts with similar magnesium oxide,

[1]Department of Applied Geology, The Institute for Geoscience Research (TIGeR), Centre for Exploration Targeting – Curtin node, Australian Research Council Centre of Excellence for Core to Crust Fluid Systems, Curtin University, GPO Box U1987, Perth, Western Australia 6845, Australia. [2]Laboratory for Crustal Petrology, Department of Geology, University of Maryland, College Park, Maryland 20742-4211, USA. [3]Geological Survey of Western Australia, 100 Plain Street, East Perth, Western Australia 6004, Australia.

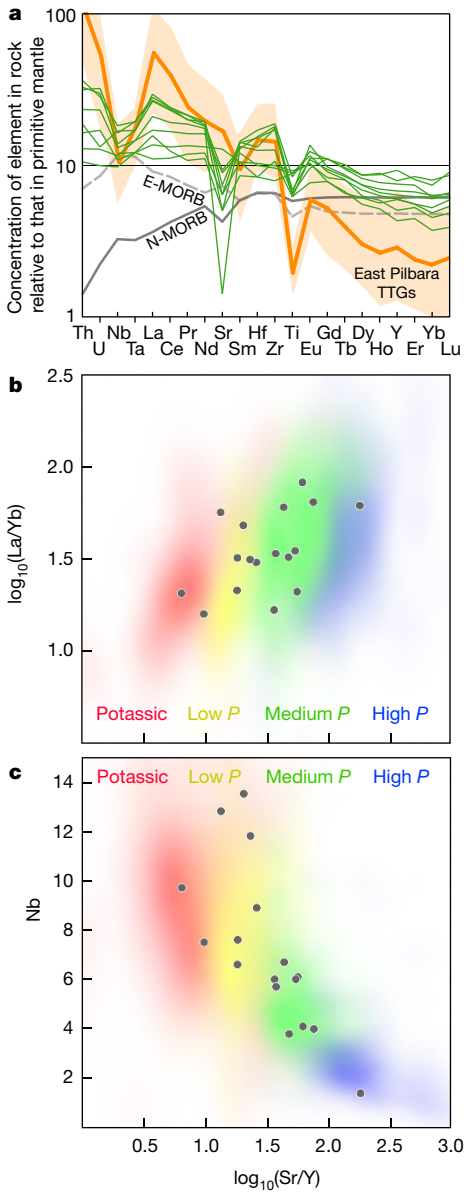

Figure 1 | Trace-element geochemistry. a, Concentration of selected trace elements in uncontaminated Coucal basalts (green) and Palaeoarchaean East Pilbara TTGs (pale orange field, with average composition in darker orange; $n = 15$) relative to primitive mantle[28]. For reference, the compositions of N-MORB and E-MORB[28] are also shown. **b**, **c**, log(La/Yb) versus log(Sr/Y) (**b**), and absolute Nb concentrations versus log(Sr/Y) (**c**) for Palaeoarchaean East Pilbara TTGs (grey dots), superimposed on smoothed kernel density estimates of Archaean TTGs and potassic granitoids worldwide[10].

chromium and nickel contents[4] (Fig. 1a). Pronounced negative anomalies are evident for niobium (and tantalum), strontium and titanium. Although a third of the Coucal basalts show evidence for crustal contamination, most have low thorium/caesium (Th/Cs) ratios (averaging 0.05), Th/Nb ratios (averaging 0.18) and La/Nb ratios (averaging 1.5), within the ranges seen in basalts considered to be free of substantial crustal influence[22,23] (Extended Data Fig. 1). The true basaltic members (with silica contents being less than 52 wt%) are not primary mantle melts (magnesium oxide = 6.1–3.1 wt%; Mg# ($100Mg/(Mg + Fe^{2+})$) = 47–30). Given that their trace-element enrichments cannot be attributed to crustal assimilation or to fractional crystallization, it has been proposed that the Coucal basalts originated in a source that was already enriched, or not yet depleted, in crustal components[4].

Palaeoarchaean TTGs (3.47–3.30 Gyr old; average silica content is 69 wt%; potassium oxide/sodium oxide ratio = 0.40; Sr/Y ratio = 35) from the East Pilbara Terrane (Fig. 1a and Extended Data Table 2) are the likely melt products derived from Coucal-like basalts. These TTGs have strongly fractionated trace-element compositions (that is, higher Th/Yb ratios and LREE/HREE ratios), but show depletions in niobium and titanium (but not strontium), rather like the Coucal basalts. Notably, almost all Palaeoarchaean East Pilbara TTGs have trace-element compositions that correspond to MP- and LP-TTGs (Fig. 1b, c)[10].

Figure 2 shows a pressure (P)–temperature (T) phase diagram calculated for the average composition of uncontaminated Coucal basalts ($n = 10$), assuming an $Fe^{3+}/\Sigma Fe$ of 0.1 (ref. 24) and a water content (4.7 mol%) that allows minimal water-saturated melting (see Extended Data Fig. 2 for the full phase diagram). Within the P–T window of interest (0.35–1.35 GPa, 630–1,000 °C), substantial melting begins with fluid-absent reactions that consume biotite, hornblende and quartz, producing around 15% melt as biotite is exhausted, and a total of 25–30% melt as hornblende (±quartz) is exhausted at 800–870 °C (Fig. 2). Above these temperatures, melting continues by consumption of anhydrous minerals, decreasing the water content of the melt. At relatively low pressures (yellow fields in Fig. 2), neither garnet nor rutile is predicted to be stable; at intermediate pressures (green fields), garnet is stable without rutile; at high pressures (blue fields), garnet and rutile co-exist. These fields correspond to the LP-TTG, MP-TTG and HP-TTG subdivisions of ref. 10, although plagioclase is predicted to be stable throughout the P–T window of interest, consistent with experiments on quartz-rich amphibolite starting compositions[17]. Notably, we calculate that garnet—which defines the lower pressure limit for MP-TTGs—is stable in the average Coucal basalt at pressures that are much lower (by up to 0.8 GPa) than suggested from experimental studies of melting in amphibolite[10,17].

The apparent geothermal gradient recorded by post-Mesoarchaean metamorphic rocks (those that formed after 2.8 billion years ago) is a function of the geodynamic setting in which they formed (for example, through subduction or accretionary/collisional orogenesis)[25]. Superimposed on Fig. 2 are linear apparent geotherms ranging upwards from 500 °C GPa^{-1}—values that encompass more than 95% of the data from Archaean metamorphic rocks worldwide[25] (Extended Data Fig. 3). Also shown are the P–T conditions of markers that represent partially molten, hydrated basalt formed in non-uniformitarian tectonic settings in models of Archaean geodynamics[9]. These settings include delamination and dripping of the lower crust into the mantle[2,15], local thickening of crust either side of upwelling mantle, and small-scale crustal overturns, all of which are predicted to produce substantial volumes of felsic (TTG) magmas[9].

To illustrate the changing composition of melts and co-existing minerals, we model the prograde evolution of the average Coucal basalt along the 900 °C GPa^{-1} geotherm (thick dashed line in Fig. 2), for which all melts in excess of 5% are predicted to have formed in equilibrium with garnet but not with rutile (that is, MP-TTGs; Figs 2, 3a and Extended Data Table 3). Corresponding data for apparent geotherms of 700 °C GPa^{-1} and 1,100 °C GPa^{-1} are shown in Extended Data Figs 4, 5 and Extended Data Table 3. The calculated compositions of melts (normalized on an anhydrous basis) formed by 5%, 10%, 15%, 20%, 25%, 30% and 40% (mol%, which approximates vol%) equilibrium melting in a closed system are shown in Fig. 3b, along with the average normalized compositions of Archaean LP-, MP- and HP-TTGs and potassic rocks worldwide[10] (see also Extended Data Table 4).

At low melt fractions (5–10%), the calculated melts are water-rich and granitic, with K_2O/Na_2O ratios greater than 0.8 (Fig. 2). At 20% melting, the calculated K_2O/Na_2O ratio (0.54) of the melt is similar to the upper range observed in TTGs, and at 30% melting this ratio (0.38) is very close to the average measured value in TTGs[10]. The major oxide composition of the average East Pilbara TTG shows remarkable correspondence with average LP- and MP-TTGs worldwide (Fig. 3b).

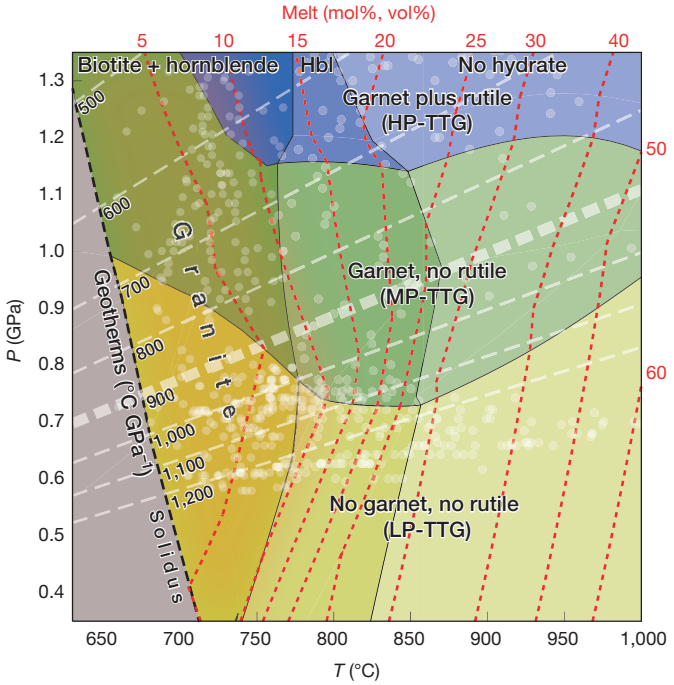

Figure 2 | Phase equilibria modelling. Simplified *P*–*T* phase diagram for an average uncontaminated Coucal basalt ($n = 10$), using an $Fe^{3+}/\Sigma Fe$ ratio of 0.1 (ref. 24) and a water content just sufficient to saturate the solidus at 1.0 GPa. The red dashed lines show the proportion of melt (mol% on a one-oxide basis, approximating vol%); at low melt fractions (<10%), the melts are granitic. For higher-melt fractions, the yellow, green and blue fields show the stability of LP-, MP- and HP-TTGs[10].The white dashed lines represent linear geotherms (°C GPa^{-1}), with the 900 °C GPa^{-1} geotherm emboldened. The white dots show the *P*–*T* conditions of markers that represent partially molten, hydrated basalt formed in non-uniformitarian tectonic settings in a numerical model of Archaean geodynamics[9].

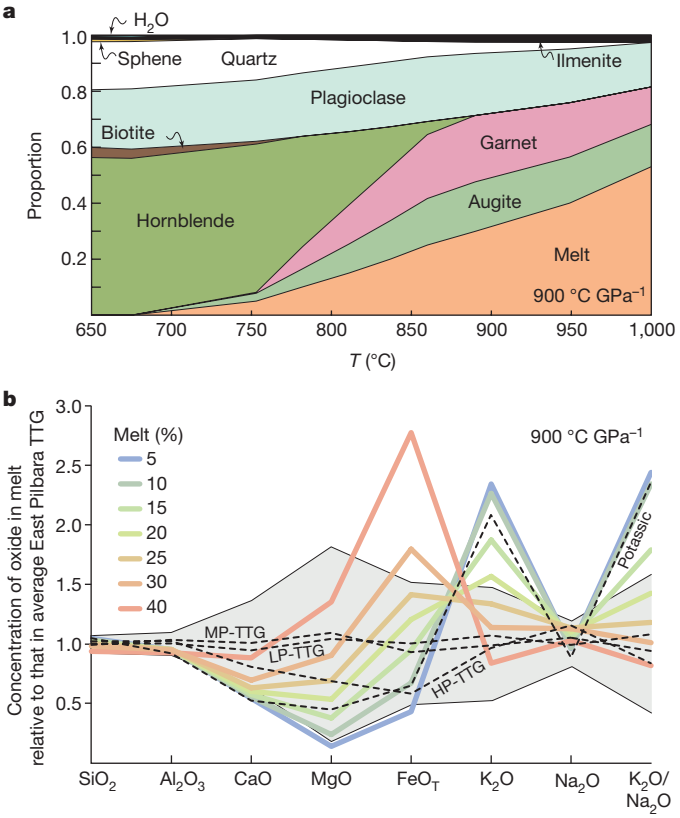

Figure 3 | For the average Coucal basalt, a plot of calculated modal proportions for melting along an apparent geotherm of 900 °C GPa^{-1}, and a comparison of calculated melt compositions with natural TTGs. **a**, Changing abundance (mode) of phases along an apparent geotherm of 900 °C GPa^{-1} for the average Coucal basalt. **b**, Calculated composition of melt produced from the average Coucal basalt at various melt fractions (5–40%), normalized to the average Palaeoarchaean East Pilbara TTG, along a geotherm of 900 °C GPa^{-1}. The grey shaded region shows the 2σ envelope on the average Palaeoarchaean East Pilbara TTG data. Also shown are the global average compositions of TTGs and potassic granitoids[10] (dashed lines). FeO_T is the total Fe oxide content considering all Fe as Fe^{2+}.

The calculated composition of melt produced from the average Coucal basalt fits best with East Pilbara TTG compositions at a modelled melt fraction of about 25% (Fig. 3b), consistent with existing mass balance constraints[5]. When using published partition coefficients[15,26,27] (Extended Data Table 5) and the predicted melt residua (Fig. 3a and Extended Data Table 3), trace-element modelling of the calculated melt compositions along the 900 °C GPa^{-1} geotherm generally shows good correspondence with the composition of the average East Pilbara TTG (Fig. 4). The fit is least good for zirconium, for which concentrations in the modelled melts are up to twice those of the average East Pilbara TTG. The reasons for this are not clear, but may reflect heterogeneities in the inferred source rocks—the Coucal basalts—in which zirconium contents vary by a factor of three (Extended Data Table 1).

Despite the major-element composition of the average Coucal basalt being broadly similar to that of N-MORB, it contains only about half of the magnesium oxide (4.0 wt% versus 8.3 wt% on an anhydrous basis) and has an Mg# of 35—lower than that of any of the amphibolite starting materials used in the experiments that underpin the threefold baric subdivision of TTGs (Mg# = 71–38)[10,17]. Calculated phase equilibria show that the low Mg# results in the stabilization of garnet and rutile at pressures of 0.7–0.8 GPa and 1.1–1.2 GPa, respectively—much lower than in the experiments. These pressures, equivalent to depths of around 20–35 km in mafic crust (Fig. 2), correspond to the lower levels of the thick plateau-like crust that would be predicted if mantle temperatures were considerably warmer in the Archaean eon than at present[2,6,7,15].

Our phase equilibria modelling demonstrates that the Palaeoarchaean East Pilbara TTGs could have been produced from 20–30% melting of a Coucal basaltic source along apparent geotherms of 700 °C GPa^{-1} or warmer (Fig. 2). Those TTGs with compositions corresponding to LP-TTGs (Fig. 1b, c) are consistent with apparent geotherms of greater than 1,100 °C GPa^{-1} (Fig. 2). These apparent geotherms are much warmer than those recorded in Neoproterozoic and younger metamorphic rocks from subduction zones (being less than 375 °C GPa^{-1}; ref. 25), but match well with apparent geotherms recorded in other Archaean metamorphic rocks, most of which exceed 700 °C GPa^{-1} (ref. 25; Extended Data Fig. 3).

Major- and trace-element compositions show that the Coucal basalts are not primary mantle melts[4]. Negative anomalies in niobium and titanium indicate source rocks with residual hornblende, rutile and/or ilmenite[12,26], but the lack of depletion in HREEs argues against the presence of residual garnet (Fig. 1a). Such patterns are consistent with source rocks that contained much more magnesium and had a much higher Mg#, requiring at least a two-stage process for production of the Coucal basalts. These observations are important, in that they suggest that the 'arc-like' trace-element signature evident in the Palaeoarchaean TTGs (Fig. 1a) was inherited through melting of the Coucal basalts. Further, our results require a protracted multigenerational process, from partial melting of the mantle to production of the first TTG magmas. This multistep melting process is not consistent with subduction, as shown by the contrast with the formation of modern-day adakites, which are thought to represent direct partial melting (together with subduction) of primary-mantle-derived crust[14]. Approximate ages of mantle melting, estimated using the samarium–neodymium isotopic

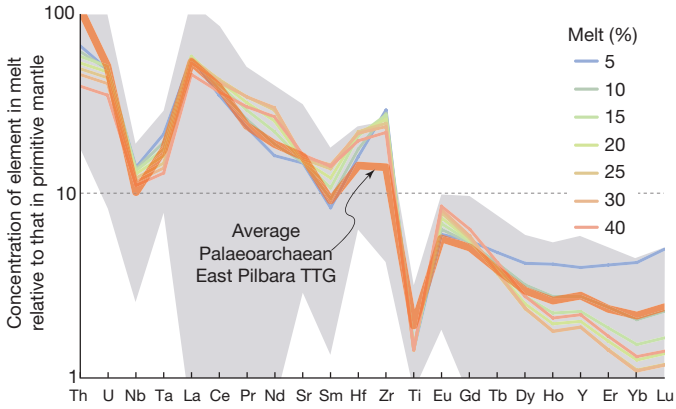

Figure 4 | Trace-element modelling. Normalized (against primitive mantle) concentration of selected trace elements in the average Palaeoarchaean East Pilbara TTG (orange), compared with the composition of modelled melts of the average Coucal basalt at various melt fractions (5–40%). The grey shaded region shows the 2σ uncertainties on the average East Pilbara TTG.

system for rocks of the Warrawoona Group, are around 3.8 Gyr, assuming a first-stage $^{147}Sm/^{144}Nd$ ratio of 0.18, consistent with a mafic source. As the earliest East Pilbara TTG rocks are around 3.5 billion years old, these data suggest a period of about 300 million years between the production of primary mafic/ultramafic crust and the formation of stable continental crust. This is sufficient time for several cycles of intracrustal melting of evolving source materials, including recycling of the dense melt residua through delamination into the mantle[2,15], and implies that TTGs had not only parents but also grandparents, and possibly great-grandparents before them.

The results of our phase equilibria modelling show that the residual mineral assemblages required by the composition of Palaeoarchaean TTGs could have stabilized in mafic source regions at much lower pressures than previously thought. An apparent geothermal gradient of more than 700 °C GPa^{-1} and temperatures of 850–900 °C may have resulted in widespread melting of Coucal-like basalts, and could thus account for the production of most of the Palaeoarchaean TTGs in the East Pilbara Terrane. These geotherms are attained in the lower levels of plateau-like mafic crust that would be predicted if Archaean mantle temperatures were considerably warmer than present[2,6,7], and are consistent with numerical simulations investigating Archaean geodynamics and the generation of TTGs[9]. Melt compositions are controlled by several factors—principally source-rock mineralogy and the conditions and extent of partial melting—and are unlikely to be unique to any particular geodynamic setting. The arc-like geochemical signature of many Archaean rocks does not require that they formed in arcs. Hence subduction was not required to produce TTGs in the early Archaean eon.

Online Content Methods, along with any additional Extended Data display items and Source Data, are available in the online version of the paper; references unique to these sections appear only in the online paper.

Received 8 September 2016; accepted 5 January 2017.
Published online 27 February 2017.

1. Condie, K. C. & Pease, V. *When Did Plate Tectonics Begin On Planet Earth?* 7th edn (Geol. Soc. Am., 2008).
2. Johnson, T. E., Brown, M., Kaus, B. J. P. & VanTongeren, J. A. Delamination and recycling of Archaean crust caused by gravitational instabilities. *Nat. Geosci.* **7,** 47–52 (2013).
3. Rapp, R. P., Shimizu, N. & Norman, M. D. Growth of early continental crust by partial melting of eclogite. *Nature* **425,** 605–609 (2003).
4. Smithies, R. H., Champion, D. C. & Van Kranendonk, M. J. Formation of Paleoarchean continental crust through infracrustal melting of enriched basalt. *Earth Planet. Sci. Lett.* **281,** 298–306 (2009).
5. Zegers, T. E. & van Keken, P. E. Middle Archean continent formation by crustal delamination. *Geology* **29,** 1083–1086 (2001).
6. Herzberg, C., Condie, K. & Korenaga, J. Thermal history of the Earth and its petrological expression. *Earth Planet. Sci. Lett.* **292,** 79–88 (2010).
7. Herzberg, C. & Rudnick, R. Formation of cratonic lithosphere: an integrated thermal and petrological model. *Lithos* **149,** 4–15 (2012).
8. Korenaga, J. Urey ratio and the structure and evolution of Earth's mantle. *Rev. Geophys.* **46,** RG2007 (2008).
9. Sizova, E., Gerya, T., Stüwe, K. & Brown, M. Generation of felsic crust in the Archean: a geodynamic modeling perspective. *Precambr. Res.* **271,** 198–224 (2015).
10. Moyen, J. F. The composite Archaean grey gneisses: petrological significance, and evidence for a non-unique tectonic setting for Archaean crustal growth. *Lithos* **123,** 21–36 (2011).
11. Rapp, R. P. & Watson, E. B. Dehydration melting of metabasalt at 8–32 kbar: implications for continental growth and crust-mantle recycling. *J. Petrol.* **36,** 891–931 (1995).
12. Foley, S., Tiepolo, M. & Vannucci, R. Growth of early continental crust controlled by melting of amphibolite in subduction zones. *Nature* **417,** 837–840 (2002).
13. Martin, H. The Archean grey gneisses and the genesis of continental crust. *Dev. Precamb. Geol.* **11,** 205–259 (1994).
14. Smithies, R. H. The Archaean tonalite-trondhjemite-granodiorite (TTG) series is not an analogue of Cenozoic adakite. *Earth Planet. Sci. Lett.* **182,** 115–125 (2000).
15. Bédard, J. H. A catalytic delamination-driven model for coupled genesis of Archaean crust and sub-continental lithospheric mantle. *Geochim. Cosmochim. Acta* **70,** 1188–1214 (2006).
16. Willbold, M., Hegner, E., Stracke, A. & Rocholl, A. Continental geochemical signatures in dacites from Iceland and implications for models of early Archaean crust formation. *Earth Planet. Sci. Lett.* **279,** 44–52 (2009).
17. Moyen, J. F. & Stevens, G. in *Archean Geodynamics and Environments* (eds Benn, K., Mareschal, J.-C. & Condie, K. C) 149–175 (Am. Geophys. Union, 2006).
18. Martin, H. & Moyen, J.-F. Secular changes in tonalite-trondhjemite-granodiorite composition as markers of the progressive cooling of Earth. *Geology* **30,** 319–322 (2002).
19. Green, E. C. R. *et al.* Activity-composition relations for the calculation of partial melting equilibria in metabasic rocks. *J. Metamorph. Geol.* **34,** 845–869 (2016).
20. Van Kranendonk, M. J., Hickman, A. H., Smithes, R. H. & Nelson, D. R. Geology and tectonic evolution of the Archean North Pilbara Terrain, Pilbara Craton, Western Australia. *Econ. Geol.* **97,** 695–732 (2002).
21. Van Kranendonk, M. J. *et al.* Making it thick: a volcanic plateau origin of Palaeoarchean continental lithosphere of the Pilbara and Kaapvaal cratons. *Geol. Soc. Spec. Publ.* **389,** 83–111 (2015).
22. Kerrich, R., Polat, A., Wyman, D. & Hollings, P. Trace element systematics of Mg-, to Fe-tholeiitic basalt suites of the Superior Province: implications for Archean mantle reservoirs and greenstone belt genesis. *Lithos* **46,** 163–187 (1999).
23. Condie, K. C. Incompatible element ratios in oceanic basalts and komatiites: tracking deep mantle sources and continental growth rates with time. *Geochem. Geophys. Geosyst.* **4,** 1–28 (2003).
24. Berry, A. J. *et al.* Oxidation state of iron in komatiitic melt inclusions indicates hot Archaean mantle. *Nature* **455,** 960–963 (2008).
25. Brown, M. The contribution of metamorphic petrology to understanding lithosphere evolution and geodynamics. *Geosci. Frontiers* **5,** 553–569 (2014).
26. Xiong, X. *et al.* Partitioning of Nb and Ta between rutile and felsic melt and the fractionation of Nb/Ta during partial melting of hydrous metabasalt. *Geochim. Cosmochim. Acta* **75,** 1673–1692 (2011).
27. McKenzie, D. & O'Nions, R. K. Partial melt distributions from inversion of rare earth element concentrations. *J. Petrol.* **32,** 1021–1091 (1991).
28. Sun, S.-s. & McDonough, W. F. Chemical and isotopic systematics of oceanic basalts: implications for mantle composition and processes. *Geol. Soc. Spec. Publ.* **42,** 313–345 (1989).

Supplementary Information is available in the online version of the paper.

Acknowledgements We acknowledge financial support from The Institute of Geoscience Research (TIGeR) at Curtin University. R.H.S. publishes with the permission of the Executive Director, Geological Survey of Western Australia.

Author Contributions T.E.J. conceived the project and performed the phase equilibria calculations. N.J.G. undertook the trace-element modelling. All authors analysed the data and contributed to writing the paper.

Author Information Reprints and permissions information is available at www.nature.com/reprints. The authors declare no competing financial interests. Readers are welcome to comment on the online version of the paper. Correspondence and requests for materials should be addressed to T.E.J. (tim.johnson@curtin.edu.au).

Reviewer Information *Nature* thanks J. Bédard, R. Rapp and the other anonymous reviewer(s) for their contribution to the peer review of this work.

METHODS

Coucal basalt geochemistry. The Coucal basalts ($n = 15$; Extended Data Table 1) form a tholeiitic series that is characterized by substantial enrichment in incompatible trace elements relative to E-MORB, N-MORB, and other Pilbara Supergroup basalts with similar MgO, Cr and Ni contents (Fig. 1a)[4]. Pronounced negative anomalies are evident for Nb (and Ta), Sr and Ti. Depletions in Sr are accompanied by similar depletions in Ba and Rb, but not Eu; and Sr/Eu decreases with increasing content of volatile species (on the basis of analytical loss on ignition). This suggests that the destructive alteration of feldspar, under relatively oxidizing conditions, has led to an underestimate in the concentrations of many fluid-mobile trace elements. Of the Coucal basalts, a group ($n = 5$) that defines a trend to higher La/Nb and Th/Nb ratios with increasing silica and decreasing Ti/Gd is thought to have assimilated felsic crust[4] (Extended Data Fig. 1) and was excluded. The remaining ten samples have low Th/Ce (average = 0.05), Th/Nb (average = 0.18) and La/Nb (average = 1.5) ratios, within the range for basalts considered to be free of major crustal influence[22,23].

Phase equilibria modelling. Phase equilibria modelling was undertaken in the ten-component Na_2O–CaO–K_2O–FeO–MgO–Al_2O_3–SiO_2–H_2O–TiO_2–O (NCKFMASHTO) chemical system for an average uncontaminated Coucal basalt ($n = 10$), with a composition, in terms of the mol% of the oxides Na_2O–CaO–K_2O–FeO–MgO–Al_2O_3–SiO_2–H_2O–TiO_2–O, of 2.954, 8.560, 0.360, 11.486, 6.221, 8.910, 54.929, 4.734, 1.269, 0.578 (see also Extended Data Table 1). Calculations used THERMOCALC version 3.45i (ref. 29) and the internally consistent thermodynamic data set ds63 (ref. 30; updated 5 January 2015). Activity–composition solution models were as follows: tonalitic melt, augite and hornblende[19] with a reduced Darken's quadratic formulation (DQF) value for the glaucophane end-member of −3 kJ mol^{-1} from 0 kJ mol^{-1}; garnet, orthopyroxene, biotite and chlorite[31]; olivine and epidote[30]; magnetite–spinel[32]; ilmenite–hematite[33]; C$^-$1 plagioclase and K-feldspar[34]; and muscovite–paragonite with a reduced DQF value for the margarite end-member of 5 kJ mol^{-1} from 6.5 kJ mol^{-1}. Pure phases include quartz, rutile, sphene (titanite), and aqueous fluid (H_2O). The results are shown in an isochemical P–T phase diagram, or pseudosection, between 0.35 GPa and 1.35 GPa, and between 630 °C and 1,000 °C (Extended Data Fig. 2). The H_2O content in the modelled composition was fixed to be just sufficient to saturate the solidus at 1.0 GPa (producing less than 1 mol% H_2O-saturated melt). The quantity of H_2O-saturated melt is less than 5 mol% at all modelled pressures in excess of 0.4 GPa, but greater than 5 mol% at pressures below this (Fig. 2 and Extended Data Fig. 2). Assemblage fields are labelled with stable phases, in which abbreviations are as follows: melt (L), garnet (g), augite (aug), orthopyroxene (opx), hornblende (hb), biotite (bi), magnetite (mt), ilmenite (ilm), plagioclase (pl), K-feldspar (ksp), muscovite (mu), quartz (q), rutile (ru), sphene = titanite (sph), and aqueous fluid (H_2O). All fields contain plagioclase. The depth of shading of assemblage fields reflects increasing variance. The field with the highest variance (aug–opx–ilm–L) at high temperatures and low pressures has a variance of 7 (Extended Data Fig. 2).

The software and data files used to generate the phase diagrams can be downloaded from http://www.metamorph.geo.uni-mainz.de/thermocalc.

Trace-element modelling. For trace-element modelling (Fig. 4), we used the average uncontaminated Coucal basalt[4] as a starting composition and the calculated abundance of phases along the 900 °C GPa^{-1} geotherm at various melt fractions (Figs 2 and 3a, Extended Data Table 3). We consider the residua to contain a fixed amount (1%) of apatite, as well as an amount of zircon that was calculated from the zircon concentration in the average Coucal basalt (200 p.p.m.), the composition of the melt at the appropriate temperature (Extended Data Table 4), the melt fraction and a refined zircon solubility model[35]. The calculations predict 0.03 mol% zircon in the residua at melt fractions of 5%, 0.02 mol% at melt fractions of 10%, 0.001 mol. at melt fractions of 15%, and no zircon thereafter. Mineral/melt partition coefficients (D) are taken from the literature and tabulated in Extended Data Table 5. Most D values follow ref. 15 (wherein the values were calculated for anatexis of metabasites), with some important modifications. For the modelled hornblende compositions (Mg# = 37–51), we use $D_{Nb} = 0.8$ and $D_{Ta} = 0.38$ (ref. 27), to give a D_{Nb}/D_{Ta} ratio of 2.1, which is more appropriate for residua containing low-Mg amphiboles[12]. For ilmenite we use values for D_{Nb} and D_{Ta} of 45 and 40, respectively[26], and for D_{Ti} a value of 150 (ref. 36).

Data availability. The data supporting the findings of this study are available within the paper (including Methods and Extended Data); data in Extended Data Tables 1 and 2 are provided as Supplementary Information.

29. Powell, R. & Holland, T. J. B. An internally consistent dataset with uncertainties and correlations: 3. Applications to geobarometry, worked examples and a computer program. *J. Metamorph. Geol.* **6,** 173–204 (1988).
30. Holland, T. J. B. & Powell, R. An improved and extended internally consistent thermodynamic dataset for phases of petrological interest, involving a new equation of state for solids. *J. Metamorph. Geol.* **29,** 333–383 (2011).
31. White, R. W., Powell, R., Holland, T. J. B., Johnson, T. E. & Green, E. C. R. New mineral activity-composition relations for thermodynamic calculations in metapelitic systems. *J. Metamorph. Geol.* **32,** 261–286 (2014).
32. White, R. W., Powell, R. & Clarke, G. L. The interpretation of reaction textures in Fe-rich metapelitic granulites of the Musgrave Block, Central Australia: constraints from mineral equilibria calculations in the system. *J. Metamorph. Geol.* **20,** 41–55 (2002).
33. White, R., Powell, R., Holland, T. & Worley, B. The effect of TiO_2 and Fe_2O_3 on metapelitic assemblages at greenschist and amphibolite facies conditions: mineral equilibria calculations in the system K_2O-FeO-MgO-Al_2O3-SiO_2-H_2O-TiO_2-Fe_2O_3. *J. Metamorph. Geol.* **18,** 497–511 (2000).
34. Holland, T. & Powell, R. Activity–composition relations for phases in petrological calculations: an asymmetric multicomponent formulation. *Contrib. Mineral. Petrol.* **145,** 492–501 (2003).
35. Boehnke, P., Watson, E. B., Trail, D., Harrison, T. M. & Schmitt, A. K. Zircon saturation re-revisited. *Chem. Geol.* **351,** 324–334 (2013).
36. Stimac, J. & Hickmott, D. Trace-element partition coefficients for ilmenite, orthopyroxene and pyrrhotite in rhyolite determined by micro-PIXE analysis. *Chem. Geol.* **117,** 313–330 (1994).

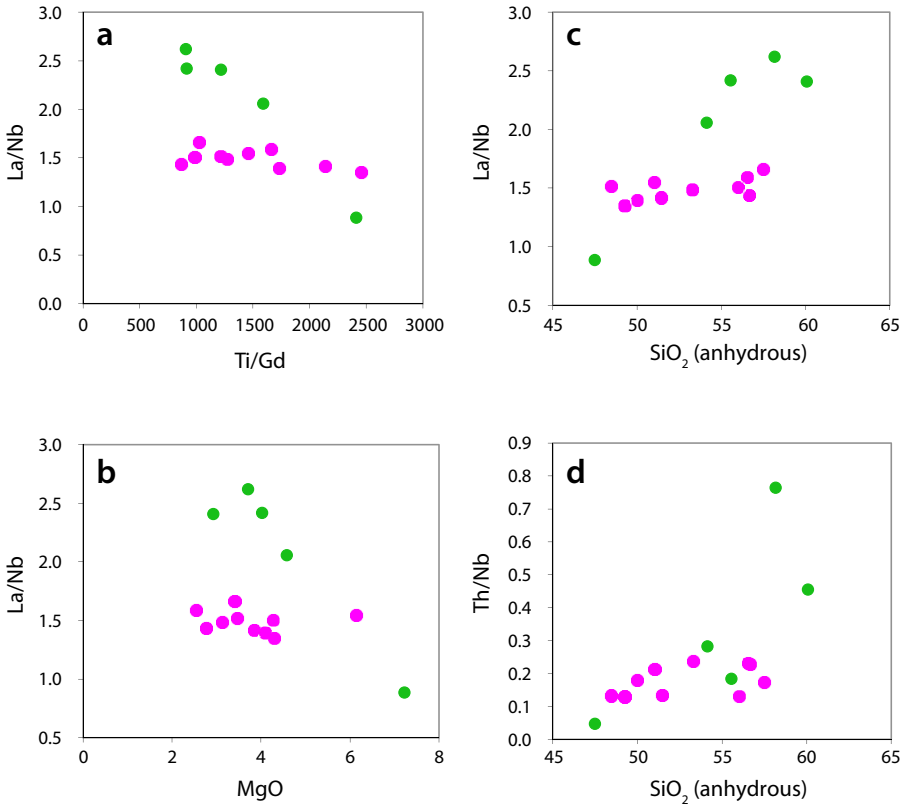

Extended Data Figure 1 | Variation diagrams for samples of the Coucal basalts. a, La/Nb versus Ti/Gd ratios. **b**, La/Nb ratios versus MgO (wt%) concentration. **c**, La/Nb ratios versus wt% silica (SiO_2, anhydrous) concentrations. **d**, Th/Nb ratios versus wt% SiO_2 (anhydrous) concentrations. Five samples (green dots) that define a trend to higher La/Nb and Th/Nb ratios with increasing SiO_2 levels and decreasing Ti/Gd ratios are thought to have undergone assimilation of felsic crust[4] and were excluded from subsequent modelling. The remaining ten samples (pink dots), with low Th/Nb and La/Nb ratios, are considered to be free of major crustal influence[22,23].

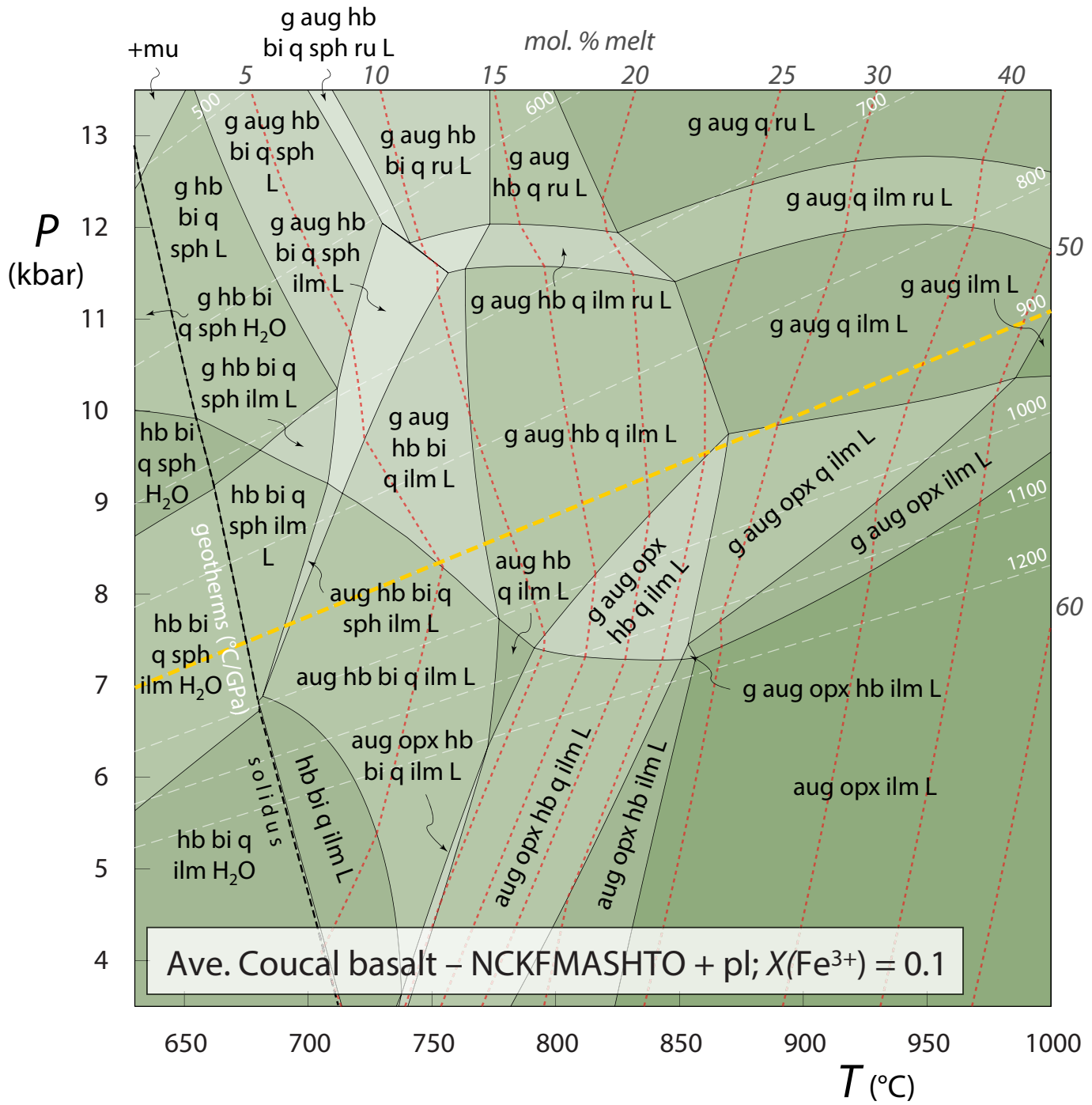

Extended Data Figure 2 | Full phase diagram for the average Coucal basalt. Full pressure–temperature (*P*–*T*) pseudosection for the average uncontaminated Coucal basalt ($n = 10$), using an $Fe^{3+}/\Sigma Fe$ ratio of 0.1 (ref. 24) and a water content just sufficient to saturate the solidus at 1.0 GPa. The red dashed lines show melt proportions as mol% on a one-oxide basis to approximate vol%. The white dashed lines show linear geotherms in °C per gigapascal. The 900 °C GPa^{-1} geotherm discussed in detail in the text, is shown in yellow. This diagram forms the basis for the simplified version shown in Fig. 2. aug, augite; bi, biotite; g, garnet; hb, hornblende; H_2O, aqueous fluid; ilm, ilmenite; ksp, K-feldspar; L, melt; mt, magnetite; muscovite (mu); opx, orthopyroxene; pl, plagioclase; q, quartz; ru, rutile; sph, sphene = titanite.

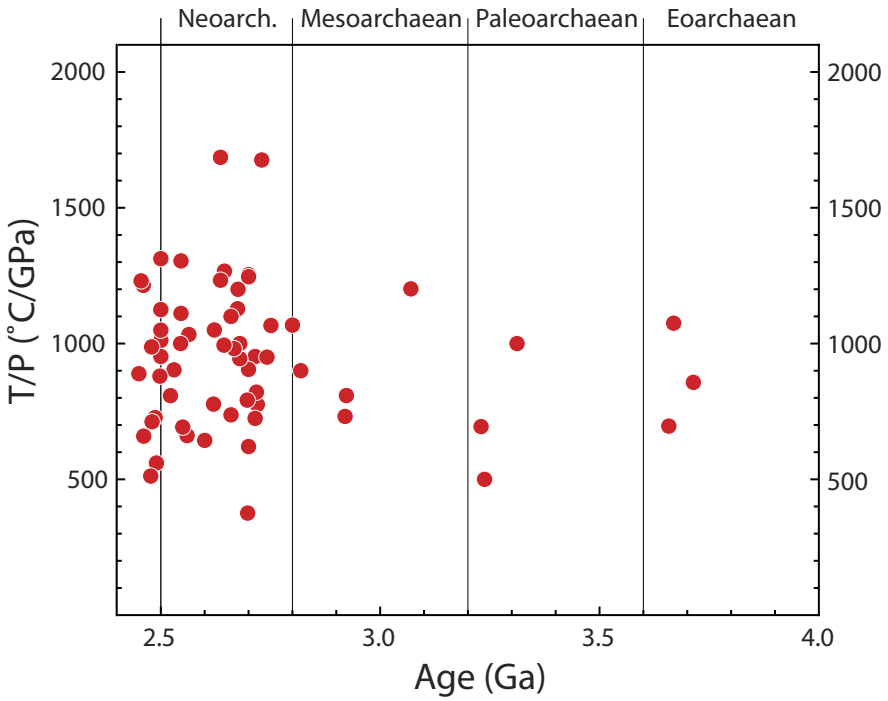

Extended Data Figure 3 | Apparent geotherms recorded in metamorphic rocks dated to 2.4 Gyr ago or older. The geotherms (*T*/*P*) are shown in units of °C per gigapascal. All but one rock of Archaean age (2.5 Gyr or older) record apparent geotherms of 500 °C GPa^{-1} or higher, and most are more than, or much more than, 700 °C GPa^{-1} (M.B. and T.E.J., manuscript in preparation). These findings are consistent with a global database of TTG compositions, 76% of which are LP- and MP-TTGs[10] (see yellow and green fields in Fig. 2).

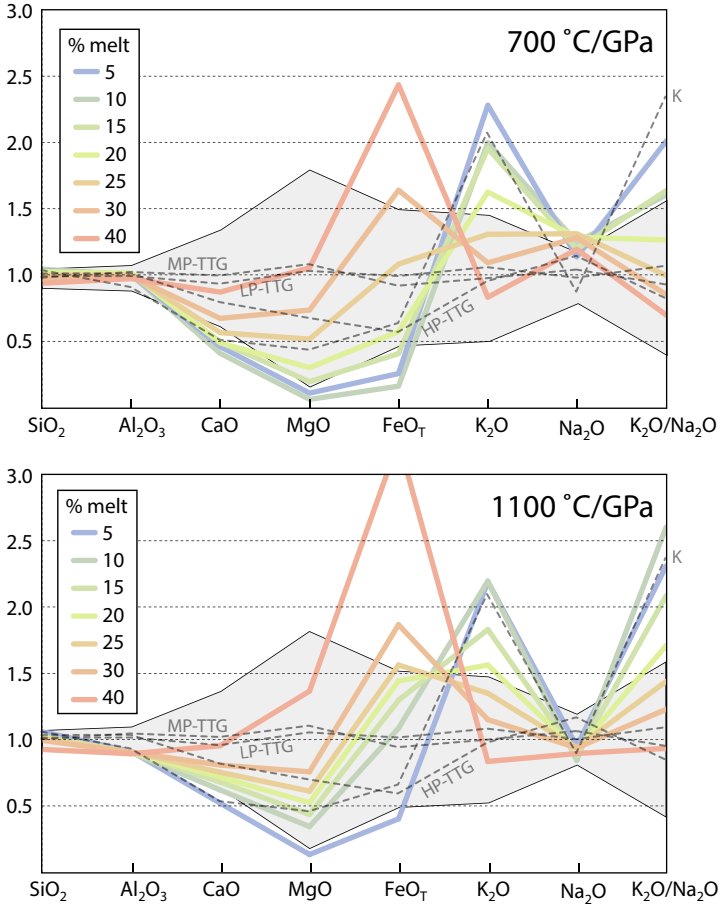

Extended Data Figure 4 | Calculated melt compositions for melting along apparent geotherms of 700 °C GPa^{-1} and 1,100 °C GPa^{-1}. Calculated composition of melt produced from the average Coucal basalt along linear geotherms of 700 °C GPa^{-1} (top) and 1,100 °C GPa^{-1} (bottom) at various melt fractions (5–40%), normalized to the average composition of Palaeoarchaean East Pilbara TTG. The grey shaded region shows the 2σ envelope on the average Palaeoarchaean East Pilbara TTG data. Also shown are the average composition of TTGs and potassic granitoids worldwide[10]. As with the 900 °C GPa^{-1} data (Fig. 3a), the modelled melt compositions fit best at melt fractions of 20–30 mol% (approximate vol%).

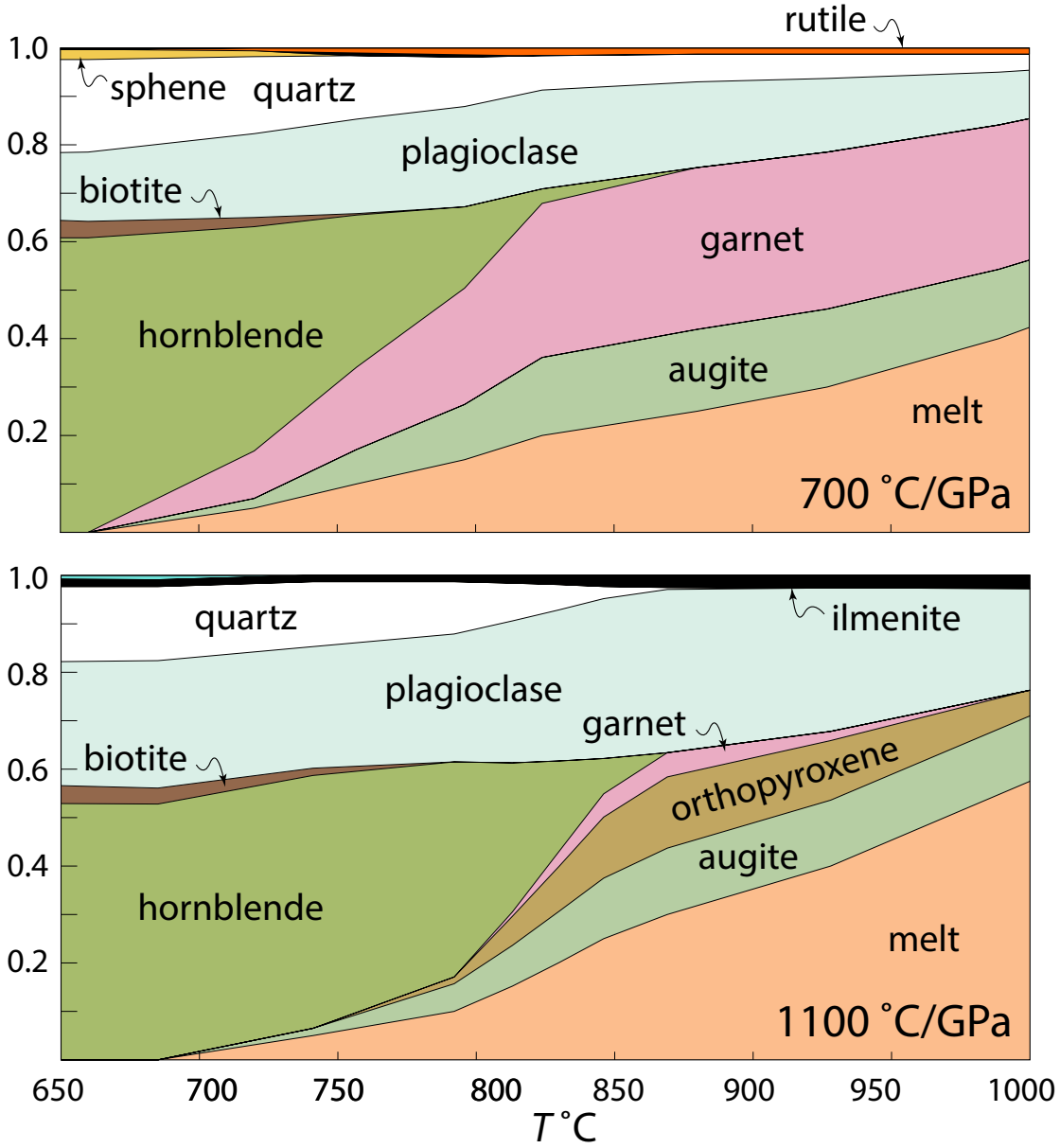

Extended Data Figure 5 | Calculated modal proportion for melting along apparent geotherms of 700 °C GPa^{-1} and 1,100 °C GPa^{-1}. Plots of modal proportions versus temperature (also known as modebox diagrams) showing the changing abundance of phases, modelled along linear geotherms of 700 °C GPa^{-1} (top) and 1,100 °C GPa^{-1} (bottom). Assemblages developed along the cooler geotherm (700 °C GPa^{-1}) contain (at temperatures greater than 700 °C) abundant garnet, as well as a small quantity (<2 mol%) of suprasolidus sphene (titanite) at lower temperatures (less than 750 °C), of ilmenite at intermediate temperatures (700–860 °C), and of rutile at temperatures higher than 800 °C (that is, these assemblages are HP-TTGs). Little garnet and no rutile forms along the 1,100 °C GPa^{-1} geotherm, consistent with the formation of LP- and MP-TTGs; all of these assemblages contain a small amount (less than 2 mol%) of ilmenite, but no sphene.

Extended Data Table 1 | Major-element oxide (wt%) and trace-element (p.p.m.) bulk rock composition of Coucal basalts

Age(Ma)	3515	3515	3515	*3515*	*3515*	3515	3515	3515	*3515*	3515	3515	3515	*3515*	3515	*3515*	
Sample #	**179777**	**179780**	**179782**	***179785***	***179789***	**179790**	**179791**	**179792**	***179794***	**179806**	**179808**	**179809**	***179810***	**179813**	***179865***	**AVE.**
EASTING	717157	717066	716865	*716702*	*715895*	715873	715722	715700	*715646*	711949	731649	731668	*731709*	731761	*730221*	
NORTHING	7664736	7664492	7664216	*7663911*	*7663227*	7663258	7662818	7662882	*7662881*	7663602	7667444	7667483	*7667546*	7667853	*7668816*	
SiO2	54.52	48.26	55.85	*53.69*	*46.47*	45.85	56.60	53.44	*54.79*	51.93	44.09	47.31	*54.65*	42.12	*59.47*	**50.00**
TiO2	1.30	1.36	1.83	*1.50*	*2.00*	1.42	1.34	1.43	*1.46*	1.41	1.92	1.94	*0.76*	1.35	*1.24*	**1.53**
Al2O3	15.55	15.08	14.07	*14.70*	*14.97*	11.41	15.95	15.24	*15.80*	15.77	11.93	12.77	*16.07*	9.87	*15.26*	**13.77**
Fe2O3*	11.34	14.87	15.82	*12.74*	*15.35*	13.44	10.37	10.74	*11.64*	13.79	16.99	17.00	*7.55*	14.56	*10.28*	**13.89**
FeO	10.20	13.38	14.24	*11.46*	*13.81*	12.09	9.33	9.67	*10.47*	12.41	15.28	15.30	*6.79*	13.10	*9.25*	**12.50**
MnO	0.15	0.27	0.44	*0.24*	*0.24*	0.25	0.19	0.19	*0.24*	0.13	0.25	0.24	*0.10*	0.34	*0.13*	**0.24**
MgO	2.78	4.10	2.55	*4.58*	*7.22*	6.15	3.41	4.27	*4.02*	3.14	4.31	3.85	*3.71*	3.47	*2.93*	**3.80**
CaO	6.36	10.68	5.61	*8.59*	*9.24*	9.94	5.60	5.38	*5.79*	8.71	6.08	6.25	*5.05*	12.06	*5.46*	**7.67**
Na2O	3.38	2.06	3.10	*3.17*	*2.30*	0.04	4.67	4.23	*4.46*	2.00	3.61	2.82	*5.80*	1.83	*3.01*	**2.77**
K2O	1.09	0.62	0.22	*0.56*	*0.91*	0.96	0.53	0.54	*0.63*	1.06	0.02	0.01	*0.28*	0.17	*1.37*	**0.52**
P2O5	0.42	0.21	0.35	*0.33*	*0.14*	0.15	0.36	0.44	*0.56*	0.35	0.16	0.19	*0.13*	0.34	*0.24*	**0.30**
LOI	3.96	3.64	1.27	*0.85*	*2.20*	11.33	1.64	4.82	*1.40*	2.67	11.76	8.79	*6.45*	15.06	*1.03*	**6.49**
Total	100.85	101.13	101.10	*100.92*	*101.04*	100.94	100.66	100.73	*100.79*	100.95	101.11	101.18	*100.53*	101.17	*100.41*	**100.98**
Mg#	32.66	35.29	24.17	*41.59*	*48.24*	47.55	39.43	44.07	*40.65*	31.05	33.44	30.97	*49.32*	32.09	*36.06*	**35.07**
Cr	35	207	13	*32*	*145*	162	38	80	*61*	127	15	8	*80*	4	*6*	**68.90**
Ni	41	90	19	*24*	*172*	149	45	57	*40*	69	70	42	*51*	36	*15*	**61.80**
Sc	19	35	27	*33*	*27*	33	19	20	*19*	29	19	16	*17*	21	*19*	**23.80**
V	129	245	175	*250*	*174*	321	113	114	*102*	171	320	282	*139*	185	*157*	**205.50**
Cu	9	21	23	*10*	*62*	253	78	10	*6*	8	209	154	*5*	48	*49*	**81.30**
Zn	145	137	160	*98*	*119*	139	95	96	*90*	139	126	132	*76*	132	*113*	**130.10**
Mo	1.1	0.6	0.7	*1.2*	*0.7*	1.2	1.3	1.4	*1.3*	0.6	0.9	0.8	*0.3*	0.7	*1.6*	**0.93**
Sn	2.3	2	1.8	*1.9*	*1.4*	2.3	1	0.9	*1.3*	2.2	1.2	1.8	*3.9*	1.6	*3*	**1.71**
Rb	33.2	15.8	2.2	*14.5*	*24.4*	30.1	9.1	9.5	*11.5*	32.7	-1	-1	*6.1*	3.2	*41.4*	**13.38**
Cs	0.98	0.47	0.75	*0.45*	*0.62*	0.59	0.32	0.19	*0.23*	2.05	0.03	0.03	*0.09*	0.11	*1.5*	**0.55**
Ba	247	51	40	*76*	*94*	14	102	94	*118*	410	52	25	*64*	58	*659*	**109.30**
Sr	218	107	135.5	*196.5*	*136.7*	30	159	139.7	*173.9*	157.2	271.5	189.7	*72.9*	106.7	*192.7*	**151.43**
Ga	21.1	19.1	19.4	*19.6*	*18.8*	16.2	20.5	20.2	*20.5*	20.2	17.2	18.5	*20.4*	14.4	*20*	**18.68**
Ta	1	0.5	0.8	*0.7*	*0.5*	0.6	1.1	1.2	*1.3*	0.8	0.5	0.6	*0.9*	0.7	*0.9*	**0.78**
Nb	19.9	7.8	11.7	*9.9*	*8.6*	9.4	18	20.9	*21.2*	13.1	7	8.3	*10.2*	12.1	*11.2*	**12.82**
Ti	7799	8129	10947	*8969*	*12008*	8531	8057	8573	*8753*	8453	11510	11630	*4574*	8081	*7434*	**9171.15**
Hf	6	2.6	5.3	*4.8*	*3.2*	3.9	7.3	7.7	*8*	4.1	2.6	3.1	*5*	4.7	*6.2*	**4.73**
Zr	294	120	212	*203*	*112*	142	311	329	*331*	198	89	108	*188*	193	*232*	**199.60**
Y	55	27.2	36.2	*31*	*27.4*	29.1	43.6	47.7	*48.9*	42.4	19.7	23.1	*28.3*	34.4	*33.1*	**35.84**
Th	4.5	1.4	2.7	*2.8*	*0.4*	2	3.1	2.7	*3.9*	3.1	0.9	1.1	*7.8*	1.6	*5.1*	**2.31**
U	0.92	0.36	0.68	*0.63*	*-0.1*	0.49	0.74	0.62	*0.79*	0.6	0.21	0.27	*1.85*	0.28	*1.17*	**0.52**
Pb	5	5	4	*4*	*3*	8	3	3	*4*	6	9	11	*5*	6	*6*	**6.00**
La	28.54	10.86	18.59	*20.37*	*7.62*	14.52	29.87	31.46	*51.29*	19.45	9.43	11.76	*26.71*	18.33	*26.96*	**19.28**
Ce	57.4	22.24	41.82	*43.21*	*19.91*	34.23	63.51	71.09	*109.5*	42.7	23.6	29.82	*49.68*	41.35	*57.38*	**42.78**
Pr	7.3	2.99	5.96	*5.96*	*3.29*	5.2	8.48	9.59	*14.51*	5.54	3.74	4.5	*5.94*	5.57	*7.06*	**5.89**
Nd	34.14	15.1	26.45	*25.15*	*16.45*	23.86	35.26	40.09	*57.07*	26.49	18.06	21.98	*23.35*	24.68	*28.05*	**26.61**
Sm	8.18	3.81	6.43	*5.75*	*4.69*	5.95	7.61	9.02	*10.99*	6.34	4.69	5.38	*4.61*	6.28	*6.26*	**6.37**
Eu	2.058	1.294	2.084	*1.839*	*1.713*	2.299	2.307	2.493	*2.733*	1.618	1.748	1.955	*1.198*	1.877	*1.534*	**1.97**
Gd	8.92	4.69	6.57	*5.64*	*4.98*	5.85	7.84	8.68	*9.57*	6.62	4.68	5.44	*5.04*	6.64	*6.1*	**6.59**
Tb	1.33	0.71	1.1	*0.92*	*0.87*	0.94	1.3	1.48	*1.55*	1.05	0.73	0.88	*0.85*	1.03	*0.97*	**1.06**
Dy	8.51	4.52	6.38	*5.51*	*5.09*	5.48	7.71	8.48	*8.51*	6.39	4.09	4.65	*4.82*	6.07	*5.86*	**6.23**
Ho	1.75	0.93	1.46	*1.15*	*1.04*	1.09	1.65	1.84	*1.9*	1.43	0.85	0.97	*1.05*	1.27	*1.28*	**1.32**
Er	4.79	2.68	4.07	*3.22*	*2.67*	3	4.6	5.11	*5.17*	3.9	2.15	2.54	*3.07*	3.58	*3.75*	**3.64**
Yb	4.64	2.6	3.96	*3.14*	*2.4*	2.98	4.37	5.04	*4.98*	3.67	1.84	2.24	*3.08*	3.07	*3.46*	**3.44**
Lu	0.79	0.44	0.64	*0.48*	*0.4*	0.47	0.71	0.84	*0.82*	0.67	0.29	0.36	*0.5*	0.49	*0.56*	**0.57**

Samples in italics are those that show evidence for crustal contamination (see Extended Data Fig. 1). The average composition of the remaining (uncontaminated) ten samples is in boldface. Data are provided in Supplementary Table 1. Ma, millions of years.

Extended Data Table 2 | Major-element oxide (wt%) and trace-element (p.p.m.) bulk rock composition of Palaeoarchaean East Pilbara Terrane (EPT) TTGs

Sample	169040	169045	160211	169031	142968	142984	169028	160208	142985	169038	142962	169046	160210	142974	142981	142976	AVERAGE	*169042*
EASTING	215701	795469	791618	189900	731451	191666	782780	789699	807661	211560	743968	795310	788440	791891	204598	766668		*211150*
NORTHING	7641310	7648058	7621829	7651153	7592357	7654482	7602400	7632149	7654152	7645701	7633191	7647502	7626210	7660103	7652929	7632651		*7631923*
Al2O3	14.198	15.204	14.708	14.837	15.4	14.42	13.224	14.331	15.29	16.068	15.3	15.914	14.908	15.81	15.8	15.06	**15.03**	*15.059*
Ba	303	263	206	348	631	339	482	486	864	294	753	288	366	1008	578	903	**507.00**	*269*
Be	0.7	0.6	1.4	1	1.4	1.8	0.7	0.9	3.6	1	1.2	0.6	0.8	1	1.6	0.8	**1.19**	*0.7*
CaO	1.954	2.851	2.577	3.499	2.56	2.96	3.31	3.415	3.4	3.478	3.72	4.125	3.881	4.12	4.15	3.59	**3.35**	*2.49*
Ce	20.56	31.17	46.58	130.4	46.5	76.01	87.54	55.49	98.58	48.21	85.6	65.89	46.58	147.6	131.9	47.32	**72.87**	*27.95*
Cr	7	8	6	7	7	12	18	25	24	9	43	5	18	47	34	41	**19.44**	*8*
Cs	1.77	3.62	3.2	11.25	6.51	1.44	2.87	4.37	56.37	0.81	2.58	3.74	3.89	3.5	10	1.07	**7.31**	*1.02*
Cu	16	7	5	6	6	11	15	9	11	7	6	19	22	23	23	5	**11.94**	*8*
Dy	1.18	1.15	1.61	3.25	1.37	1.13	4.57	3.85	2.97	1.56	1.59	2.35	2.34	2.29	3.86	1.52	**2.29**	*0.45*
Er	0.62	0.66	0.7	1.38	0.7	0.53	2.62	2.09	1.56	0.87	0.73	1.21	1.36	1.2	2.01	0.78	**1.19**	*0.23*
Eu	0.465	0.619	0.722	1.398	0.798	0.752	1.186	0.993	1.425	0.617	1.116	1.105	1.019	1.587	1.727	0.927	**1.03**	*0.447*
F	249	263	370	397	678	519	667	547	1946	507	641	684	481	649	868	673	**633.69**	*304*
Fe2O3T	1.434	2.066	2.826	3.742	2.6	2.96	4.547	4.113	3.51	3.338	3.73	4.664	4.385	4.13	4.44	3.81	**3.52**	*1.577*
FeOT	1.29	1.86	2.54	3.37	2.34	2.66	4.09	3.70	3.16	3.00	3.36	4.20	3.95	3.72	4.00	3.43	**3.17**	*1.42*
FeO	0.761	1.277	1.656	2.124	1.5	1.96	2.83	2.552	1.76	1.715	1.45	2.692	2.725	2.08	2.44	1.92	**1.97**	*0.8*
Ga	19	19.4	18.8	18.9	20.5	17.3	18.5	18.5	18	21.4	17.2	19.7	19.1	17.5	19	19.7	**18.91**	*19.4*
Gd	1.6	1.53	2.52	5.53	2.04	1.92	5.31	4	4.31	1.94	2.94	3.19	2.85	3.83	5.66	2.56	**3.23**	*0.93*
Hf	2.9	2.9	4.9	7.8	3.8	5.5	5.2	5.1	4.2	4	3.3	5.3	3.8	4.9	5.5	3.3	**4.53**	*3.4*
Ho	0.25	0.25	0.3	0.61	0.24	0.19	0.96	0.78	0.55	0.34	0.28	0.49	0.5	0.43	0.69	0.28	**0.45**	*0.09*
K2O	2.356	1.461	1.429	1.273	1.66	0.89	1.999	2.162	2.51	1.707	1.76	1.444	1.858	1.65	1.87	2.03	**1.75**	*1.337*
La	10.41	15.39	28.88	70.69	23.13	39.45	50.03	31.13	44.61	26.79	45.05	38.22	26.57	73.54	62.3	22.33	**38.03**	*14.81*
LOI	0.604	0.813	1.425	0.107	1.13	3.05	2.369	1.552	0.29	1.68	0.93	0.788	2.245	0.4	0.18	3.15	**1.29**	*0.134*
Lu	0.1	0.13	0.11	0.24	0.09	0.08	0.4	0.34	0.2	0.14	0.1	0.22	0.22	0.18	0.27	0.09	**0.18**	*0.04*
MgO	0.415	0.654	0.585	0.745	0.83	0.84	1.211	1.271	1.48	1.045	1.8	1.148	1.303	2.04	1.93	1.65	**1.18**	*0.519*
MnO	0.03	0.034	0.05	0.049	0.05	0.03	0.065	0.059	0.06	0.052	0.06	0.068	0.067	0.07	0.07	0.08	**0.06**	*0.019*
Na2O	4.606	4.882	4.547	4.005	5.26	4.62	3.668	3.88	4.21	4.815	4.85	4.254	3.951	4.24	4.62	4.59	**4.44**	*5.227*
Nb	6	6.1	13.5	12.8	6	4.1	9.7	7.5	8.9	5.7	4	7.6	6.6	6.7	11.8	3.8	**7.55**	*1.4*
Nd	9.05	12.02	16.66	50.48	17.52	24.09	35.09	22.8	37.96	17.7	32.69	25.02	19.25	46.68	50.72	20.04	**27.36**	*10.69*
Ni	12	12	13	15	13	14	23	29	24	19	30	14	22	39	29	31	**21.19**	*13*
P	306	388	432	532	611	524	602	532	917	663	698	755	615	1004	1222	655	**653.60**	*353.5326*
P2O5	0.07	0.089	0.099	0.122	0.14	0.12	0.138	0.122	0.21	0.152	0.16	0.173	0.141	0.23	0.28	0.15	**0.15**	*0.081*
Pb	12.5	10.3	10.1	11.8	15.8	9.5	5.2	5	14.4	9.6	10.5	12.1	6.7	16.7	13.7	3.2	**10.44**	*7.4*
Pr	2.05	2.87	4.35	12.25	4.43	6.7	9.08	5.58	9.65	4.58	8.35	6.2	4.91	12.83	12.88	4.83	**6.97**	*2.63*
Rb	71.6	52	73.5	61.1	92.3	35	68.3	76.2	130.4	52.3	40.8	102.8	51.2	48.8	67.5	57.4	**67.58**	*33.6*
Sc	2	2	3	4	5	4	8	8	5	6	4	7	8	4	6	8	**5.25**	*3*
SiO2	74.13	71.68	71.56	71.33	70.02	69.90	69.11	68.70	68.56	67.32	67.24	66.99	66.90	66.80	66.17	65.49	**68.87**	*73.287*
Sm	1.93	1.87	2.9	7.54	2.88	3.22	6.35	4.73	6.42	2.71	4.69	4.08	3.58	6.26	7.92	3.56	**4.42**	*1.41*
Sn	1.4	1.6	1.3	1.7	2.3	2.3	2.5	1.8	4.4	1.4	1.2	2.6	1.5	2	2.5	1.5	**2.00**	*0.8*
SO3	0.032	0.052	0.027	0.031	0.03	0.04	0.032	0.028	0.1	0.035	0.04	0.045	0.029	0.03	0.15	0.05	**0.05**	*0.027*
Sr	275.7	380	176.5	217.3	431.8	366.7	202.2	208.9	458.4	403.5	628.3	278	272.9	606.9	521.6	411.2	**364.99**	*462.3*
Ta	0.9	1	0.9	1	0.6	0.6	0.9	0.9	0.8	0.6	0.4	0.4	0.6	0.7	1.1	0.3	**0.73**	*0.2*
Tb	0.23	0.22	0.32	0.7	0.28	0.24	0.78	0.58	0.63	0.29	0.34	0.44	0.39	0.51	0.8	0.33	**0.44**	*0.1*
Th	3.7	4.4	9.9	18.5	6.8	9.9	9.9	8.4	12.2	5.4	11.7	10.4	6.2	11.2	12.9	5	**9.16**	*2.5*
Ti	1181	1799	1745	2458	2218	1918	3321	3303	2758	2554	2398	3657	3369	2998	3477	2578	**2608.20**	*1540.715*
TiO2	0.197	0.3	0.291	0.41	0.37	0.32	0.554	0.551	0.46	0.426	0.4	0.61	0.562	0.5	0.58	0.43	**0.44**	*0.257*
U	1.58	0.96	1.09	1.19	1.29	0.5	1.25	1.18	0.67	0.36	2.09	1.38	0.58	1.13	0.51	1.33	**1.07**	*0.55*
V	9	21	9	15	28	15	47	44	33	34	47	45	56	26	28	70	**32.94**	*13*
Y	7.4	6.6	8.4	15.8	7.8	5.8	30.5	20.8	17.1	10.5	8.1	14.8	14.6	13.6	21.9	8.4	**13.26**	*2.5*
Yb	0.62	0.73	0.6	1.25	0.66	0.48	2.42	1.95	1.47	0.79	0.7	1.19	1.24	1.22	1.98	0.69	**1.12**	*0.24*
Zn	41	46	78	66	55	54	61	54	69	66	50	75	58	73	78	100	**64.00**	*51*
Zr	90	92	196	288	125	193	192	167	143	147	92	231	126	177	186	114	**159.94**	*115*
Age	3314	3307	3408	3430	3425	3321	3314	3300	3315	3315	3469	3310	3312	3310	3312	3469	**3351.94**	*3310*
error	6	3	7	4	4	6	4	3	5	2	2	4	3	3	4	3	**3.94**	*8*

The average composition used to compare with the modelling results excludes the single HP-TTG sample (169042; italicized). Data are provided in Supplementary Table 2.

Extended Data Table 3 | Calculated modes (in mol%, approximating vol%) of minerals and melt at various temperatures along the 900 °C GPa^{-1}, 700 °C GPa^{-1} and 1,100 °C GPa^{-1} geotherms

900° C/GPa

T (°C)	L	aug	opx	g	hb	bi	pl	q	sph	ilm	ru	H_2O
650	0.000	0.000	0.000	0.000	0.563	0.036	0.206	0.171	0.009	0.008	0.000	0.006
675	0.000	0.000	0.000	0.000	0.560	0.033	0.215	0.169	0.007	0.009	0.000	0.007
753	0.050	0.028	0.000	0.004	0.530	0.010	0.219	0.148	0.000	0.012	0.000	0.000
782	0.101	0.065	0.000	0.079	0.394	0.000	0.226	0.120	0.000	0.014	0.000	0.000
811	0.150	0.104	0.000	0.140	0.261	0.000	0.231	0.096	0.000	0.017	0.000	0.000
837	0.200	0.138	0.000	0.189	0.146	0.000	0.232	0.075	0.000	0.019	0.000	0.000
860	0.250	0.166	0.000	0.229	0.046	0.000	0.231	0.055	0.000	0.022	0.000	0.000
890	0.300	0.177	0.000	0.237	0.000	0.000	0.222	0.041	0.000	0.024	0.000	0.000
949	0.400	0.165	0.000	0.194	0.000	0.000	0.192	0.025	0.000	0.024	0.000	0.000
1000	0.531	0.151	0.000	0.134	0.000	0.000	0.159	0.001	0.000	0.025	0.000	0.000

700 °C/GPa

T (°C)	L	aug	opx	g	hb	bi	pl	q	sph	ilm	ru	H_2O
650	0.000	0.000	0.000	0.000	0.608	0.036	0.141	0.192	0.021	0.000	0.000	0.003
660	0.000	0.000	0.000	0.000	0.608	0.034	0.143	0.191	0.020	0.000	0.000	0.003
720	0.050	0.019	0.000	0.099	0.462	0.020	0.172	0.159	0.012	0.006	0.000	0.000
757	0.100	0.071	0.000	0.170	0.314	0.003	0.195	0.130	0.000	0.016	0.000	0.000
796	0.150	0.114	0.000	0.240	0.168	0.000	0.206	0.102	0.000	0.019	0.000	0.000
824	0.200	0.161	0.000	0.318	0.030	0.000	0.204	0.071	0.000	0.008	0.008	0.000
880	0.250	0.169	0.000	0.333	0.000	0.000	0.178	0.057	0.000	0.000	0.013	0.000
927	0.300	0.161	0.000	0.323	0.000	0.000	0.152	0.050	0.000	0.000	0.013	0.000
989	0.400	0.143	0.000	0.298	0.000	0.000	0.109	0.036	0.000	0.000	0.013	0.000
1000	0.423	0.139	0.000	0.292	0.000	0.000	0.100	0.033	0.000	0.000	0.013	0.000

1100 °C/GPa

T (°C)	L	aug	opx	g	hb	bi	pl	q	sph	ilm	ru	H_2O
650	0.000	0.000	0.000	0.000	0.529	0.037	0.256	0.156	0.000	0.015	0.000	0.008
685	0.000	0.000	0.000	0.000	0.528	0.033	0.263	0.153	0.000	0.014	0.000	0.009
741	0.050	0.015	0.000	0.000	0.523	0.015	0.251	0.135	0.000	0.013	0.000	0.000
792	0.100	0.057	0.014	0.000	0.444	0.000	0.264	0.108	0.000	0.013	0.000	0.000
813	0.152	0.084	0.060	0.010	0.307	0.000	0.293	0.078	0.000	0.016	0.000	0.000
830	0.201	0.106	0.093	0.032	0.186	0.000	0.312	0.052	0.000	0.019	0.000	0.000
846	0.250	0.125	0.126	0.048	0.072	0.000	0.331	0.025	0.000	0.023	0.000	0.000
869	0.300	0.136	0.148	0.050	0.000	0.000	0.337	0.004	0.000	0.025	0.000	0.000
928	0.400	0.136	0.122	0.020	0.000	0.000	0.296	0.000	0.000	0.026	0.000	0.000
1000	0.575	0.135	0.053	0.000	0.000	0.000	0.211	0.000	0.000	0.027	0.000	0.000

Extended Data Table 4 | Normalized anhydrous compositions (wt%) of the average East Pilbara Terrane (EPT) TTG, average potassic grey gneisses, LP-, MP- and HP-TTGs, and modelled melts in the NCKFMAS system

	SiO_2	Al_2O_3	CaO	MgO	FeO	K_2O	Na_2O	SUM	*K/N*
Average EPT TTG	70.49	15.36	3.45	1.21	3.19	1.73	4.56	100.00	*0.38*
Moyen averages									
POTASSIC	73.79	14.12	1.80	0.54	2.11	3.61	4.03	100.00	*0.89*
SODIC HP	71.85	15.72	2.77	0.83	1.89	1.67	5.27	100.00	*0.32*
SODIC MP	69.82	15.86	3.47	1.32	3.03	1.71	4.80	100.00	*0.36*
SODIC LP	70.46	15.39	3.25	1.25	3.27	1.85	4.52	100.00	*0.41*
900 °C/GPa									
5% melt	73.57	14.57	1.86	0.16	1.40	4.06	4.38	100.00	*0.93*
10% melt	72.75	14.55	1.90	0.28	2.18	3.92	4.41	100.00	*0.89*
15% melt	71.91	14.57	1.97	0.45	3.08	3.24	4.77	100.00	*0.68*
20% melt	71.06	14.59	2.06	0.64	3.92	2.71	5.01	100.00	*0.54*
25% melt	70.31	14.61	2.16	0.83	4.61	2.31	5.17	100.00	*0.45*
30% melt	69.05	14.52	2.39	1.09	5.86	1.97	5.13	100.00	*0.38*
40% melt	65.96	14.19	3.04	1.63	9.05	1.45	4.68	100.00	*0.31*
700 °C/GPa									
weight% anhydrous	SiO2	Al2O3	CaO	MgO	FeO	K2O	Na2O		
5% melt	73.48	15.37	1.41	0.07	0.53	3.46	5.69	100.00	*0.61*
10% melt	72.91	15.41	1.58	0.13	0.84	3.95	5.18	100.00	*0.76*
15% melt	72.38	15.52	1.70	0.24	1.32	3.39	5.46	100.00	*0.62*
20% melt	71.87	15.55	1.68	0.36	1.87	2.81	5.86	100.00	*0.48*
25% melt	70.30	15.36	1.94	0.62	3.53	2.26	5.98	100.00	*0.38*
30% melt	68.56	15.16	2.32	0.89	5.35	1.89	5.84	100.00	*0.32*
40% melt	65.99	14.92	3.00	1.27	7.94	1.44	5.44	100.00	*0.26*
1100 °C/GPa									
weight% anhydrous	SiO2	Al2O3	CaO	MgO	FeO	K2O	Na2O		
5% melt	74.63	13.99	1.79	0.16	1.31	3.79	4.33	100.00	*0.88*
10% melt	72.40	13.87	2.13	0.41	3.54	3.80	3.85	100.00	*0.99*
15% melt	71.86	13.87	2.34	0.52	4.23	3.17	4.01	100.00	*0.79*
20% melt	71.42	13.89	2.47	0.63	4.71	2.71	4.17	100.00	*0.65*
25% melt	71.03	13.93	2.59	0.74	5.09	2.34	4.28	100.00	*0.55*
30% melt	70.07	13.88	2.78	0.91	6.09	1.99	4.28	100.00	*0.47*
40% melt	65.22	13.72	3.29	1.65	10.60	1.45	4.08	100.00	*0.35*

Extended Data Table 5 | The partition coefficients (*D*) used for trace-element modelling

phase	Cpx	Opx	Plag	Amp	Biot	Garnet	Ilmen	Zircon	Apatite	Sphene	CF2
											average
Th	0.104	0.13	0.095	0.055	0.01	0.0075	0.09	62	23	0.16	2.31
U	0.032	0.089	0.091	0.05	0.1	0.024	0.09	298	25	0.14	0.52
Nb	0.007	0.01	0.239	0.8	0.085	0.04	45	50	0.05	2.2	12.82
Ta	0.028	0.126	0.053	0.38	0.107	0.08	40	50	0.05	6.55	0.78
La	0.028	0.0003	0.358	0.319	0.02	0.028	0.015	26.6	12	4.73	19.28
Ce	0.059	0.0007	0.339	0.56	0.03	0.08	0.012	23.5	15	7.57	42.78
Pr	0.116	0.0014	0.316	0.898	0.008	0.15	0.011	20	17	9	5.89
Nd	0.115	0.0028	0.289	1.32	0.03	0.222	0.01	21.7	19	12.4	26.61
Sr	0.032	0.047	4	0.389	0.1	0.019	0.0022	20	1.4	2.68	431.80
Sm	0.259	0.0085	0.237	2.09	0.04	1.43	0.009	17.7	20	14	6.37
Hf	0.208	0.246	0.069	0.781	0.023	0.431	2.4	450	16	2.43	4.73
Zr	0.125	0.031	0.078	0.417	0.023	0.7	2.3	130	16	1.92	199.60
Ti	0.473	0.5	0.078	4.03	3.5	2.63	150	10	14	67	9171.15
Eu	0.341	0.68	2.17	1.79	0.031	1.54	0.01	12.1	13	13.8	1.97
Gd	0.422	0.02	0.192	2.53	0.04	4.84	0.011	15	20	11.9	6.59
Tb	0.502	0.03	0.17	2.6	0.05	7.8	0.018	37.3	19	10	1.06
Dy	0.57	0.043	0.15	2.55	0.06	11.5	0.02	60	18	8.27	6.23
Ho	0.616	0.06	0.132	2.41	0.08	15.3	0.035	120	16.8	5.5	1.32
Y	0.603	0.054	0.138	2.47	0.07	14.1	0.037	80	17.5	5.42	35.84
Er	0.64	0.079	0.117	2.22	0.09	18.8	0.067	200	15.5	5.54	3.64
Yb	0.635	0.125	0.094	1.79	0.11	23.2	0.13	490	13	3.02	3.44
Lu	0.617	0.149	0.085	1.59	0.12	24.1	0.19	632	10	2	0.57

CORRIGENDUM

doi:10.1038/nature22385

Corrigendum: Earth's first stable continents did not form by subduction

Tim E. Johnson, Michael Brown, Nicholas J. Gardiner, Christopher L. Kirkland & R. Hugh Smithies

Nature **543,** 239–242 (2017); doi:10.1038/nature21383

In this Letter we omitted to cite a paper[1] that also used recently developed thermodynamic models[2] to predict the melting process in Archaean metabasaltic rocks. Importantly, the average enriched Archaean tholeiite used by ref. 1 as a proposed source rock[3] for tonalite–trondhjemite–granodiorite rocks has a magnesium number (Mg#) of 57, significantly higher than the average value for the CF-2 basalts (with Mg# of 35)[4]. This difference has profound implications for the results of these studies. We regret not citing ref. 1 to emphasize the clear distinction between their findings and those of our study. The original Letter has not been corrected.

1. Palin, R. M., White, R. W. & Green, E. C. R. Partial melting of metabasic rocks and the generation of tonalitic–trondhjemitic–granodioritic (TTG) crust in the Archaean: constraints from phase equilibrium modelling. *Precambr. Res.* **287,** 73–90 (2016).
2. Green, E. C. R. *et al.* Activity–composition relations for the calculation of partial melting equilibria for metabasic rocks. *J. Metamorph. Geol.* **34,** 845–869 (2016).
3. Condie, K. C. *Archaean Greenstone Belts* **434** (Elsevier, 1981).
4. Smithies, R. H., Champion, D. C. & Van Kranendonk, M. J. Formation of Paleoarchean continental crust through infracrustal melting of enriched basalt. *Earth Planet. Sci. Lett.* **281,** 298–306 (2009).